Accurate Determination of Membrane Dynamics with Line-Scan FCS

Jonas Ries, Salvatore Chiantia, and Petra Schwille*
Technical University of Dresden, Biotechnologisches Zentrum, Dresden, Germany

ABSTRACT Here we present an efficient implementation of line-scan fluorescence correlation spectroscopy (i.e., one-dimensional spatio-temporal image correlation spectroscopy) using a commercial laser scanning microscope, which allows the accurate measurement of diffusion coefficients and concentrations in biological lipid membranes within seconds. Line-scan fluorescence correlation spectroscopy is a calibration-free technique. Therefore, it is insensitive to optical artifacts, saturation, or incorrect positioning of the laser focus. In addition, it is virtually unaffected by photobleaching. Correction schemes for residual inhomogeneities and depletion of fluorophores due to photobleaching extend the applicability of line-scan fluorescence correlation spectroscopy to more demanding systems. This technique enabled us to measure accurate diffusion coefficients and partition coefficients of fluorescent lipids in phase-separating supported bilayers of three commonly used raft-mimicking compositions. Furthermore, we probed the temperature dependence of the diffusion coefficient in several model membranes, and in human embryonic kidney cell membranes not affected by temperature-induced optical aberrations.

INTRODUCTION

Fluorescence correlation spectroscopy (FCS) is a powerful tool to measure local concentrations, molecular weights, translational and rotational diffusion coefficients, chemical rate constants, association and dissociation constants, and photodynamics in vitro as well as in vivo (1,2). The measurement of fluorophores diffusing in membranes, however, meets additional challenges compared to FCS in solution, where diffusion usually is much faster. To avoid photobleaching, very low excitation powers have to be employed. To average over a sufficient number of independent events, very long continuous measurement times—at least 10^4 times larger than the diffusion time—are required, and they will finally be limited by the stability of the setup or the system. In addition to optical artifacts distorting the detection area (3), also a vertical mispositioning of the detection volume has a strong effect on the measured parameters. Although standard confocal FCS has recently been successfully applied to a variety of biological membranes (4–9), novel FCS techniques are continuously developed to simplify the experimental approach and to obtain quantitative results free from artifacts (10). An important example is scanning FCS (11–20). The basic idea is to move the detection volume with respect to the sample, and thereby reduce the residence times of the fluorophores and increase the statistical accuracy. In addition, the knowledge of the scanning parameters (e.g., scan speed) or the implementation of a two-focus cross-correlation scheme (19), avoids the calibration of the detection volume. This facilitates absolute concentration and diffusion measurements and relaxes the requirement for accurate vertical positioning of the laser focus. Due to the short residence time of the fluorophores in the detection area, higher excitation laser powers can be used without risking significant photobleaching artifacts (21). A movable detection volume can be achieved by using the scanning unit of a laser-scanning microscope (LSM). Modern LSMs, preferably with single photon detectors (usually avalanche photo diodes), can thus be readily used for scanning FCS.

Here we present a novel implementation of scanning fluorescence correlation spectroscopy with a linear scan path. As in spatiotemporal image correlation spectroscopy (22) and raster image correlation spectroscopy (17), the parallel acquisition in line-scan FCS greatly increases the statistical accuracy. However, by concentrating on one line instead of a whole frame, the higher temporal resolution and repeated sampling of the same part of the sample improves the accuracy of diffusion measurements. Compared to measurements with a stationary detection volume, the measurement time can be decreased by at least an order of magnitude.

The size of the detection area is inferred directly from the experiment and need not be determined with an additional calibration measurement. Therefore, line-scan FCS is insensitive to optical artifacts (3), optical saturation, a vertical mispositioning of the laser focus with respect to the membrane, and even a jitter in the position of the detection volume.

The slow diffusion in membranes leads to strong photobleaching in stationary FCS which results in a reduction of the apparent concentration and an increase of the apparent diffusion coefficient. In addition, the fluorophores cannot replenish efficiently due to the two-dimensional geometry. This depletion of fluorophores leads to a decrease of the concentration over time and serious distortions of the correlation curves. In line-scan FCS, on the other hand, photobleaching has virtually no effect on the measured diffusion coefficients, even for very high laser powers. The reason is the greatly reduced residence time of the molecules in the detection area due to the scanning and the distribution of the excitation power over the line. We introduce a novel scheme to fully correct for depletion due to

Submitted October 13, 2008, and accepted for publication December 3, 2008.

*Correspondence: schwille@biotec.tu-dresden.de

Editor: Lukas K. Tamm.

0006-3495/09/03/1999/10 $2.00

doi: 10.1016/j.bpj.2008.12.3888

photobleaching and therefore enable meaningful concentration and diffusion measurements even if the reservoir of fluorophores is limited, as is the case for small domains in lipid membranes.

Recently, we employed a simplified version of line-scan FCS to address significant biological problems like protein interactions with ceramide domains (23) and to investigate the effectiveness of raft-targeting drugs against Alzheimer's disease (24).

Here we demonstrate the full potential of line-scan FCS using simple but valuable examples:

First, we investigate domain-exhibiting supported bilayers. These simple lipid systems are used as models for the lipid/protein domains present in cell membranes, also called rafts (25). We measure the partition and diffusion coefficients of fluorescent lipids in three commonly used ternary mixtures of sphingomyelin, cholesterol, and dioleoylphosphatidylcholine, which all give rise to phase separation into liquid-disordered and liquid-ordered phases (26). Our results show that the partition and diffusion coefficient in the raftlike phase strongly depends on the detailed chemical composition of the bilayer. In general, we demonstrate that our technique is perfectly suitable for the quantitative study of local concentrations of membrane components. The importance of such precise determination of the affinity of membrane components to lipid domains is greatly enhanced by its biomedical significance (24).

Second, we probe the diffusion of fluorescent lipids and membrane proteins in native human embryonic kidney (HEK) plasma membrane patches, which show a complex structure compared to simple model systems. Here residual inhomogeneities would complicate the data analysis. However, they can be successfully corrected for in line-scan FCS permitting measurements even in these complex systems.

Third, we probe the temperature dependence of diffusion of lipids in simple and phase-separating model membranes and in plasma membrane patches. Studies regarding the role of temperature in determining membrane dynamics are scarce due to experimental difficulties. In contrast, our approach is not affected by problems usually connected to optical methods like temperature-induced aberrations and is therefore very solid. Assuming an Arrhenius-type dependence for the diffusion of membrane components, we were able to measure the corresponding activation energies, and thus to estimate lipid-lipid interactions.

Line-scan FCS, as demonstrated here, can be easily implemented with modern laser scanning microscopes and allows accurate and calibration-free measurements of membrane dynamics within seconds.

THEORY

In line-scan FCS the detection volume is repeatedly scanned in a linear fashion in the membrane with the velocity v (Fig. 1 *a*). The intensity traces of the line scans i can be arranged vertically to form the pseudo-image $F(x, t_i)$ (Fig. 1 *b*). Here, the horizontal axis denotes the position in the sample and the vertical axis denotes the time $t_i = i\,T$, which is an integer multiple of the scanning period T. Note that, due to the scanning, the intensity $F(x, t_i)$ is acquired at the time $t_i + x/v$. Similar to image correlation spectroscopy (22), the pseudo-image can be used to calculate the spatiotemporal correlation curve:

$$G(\xi, \tau_i) = \frac{\langle \delta F(x, t_i) \times \delta F(x + \xi, t_i + \tau_i) \rangle}{\langle F(x, t_i) \rangle^2}. \quad (1)$$

Here $\langle\rangle$ denotes the average over all positions x and scans i and $\delta F(x, t_i) = F(x, t_i) - \langle F(x, t_i) \rangle$. The value ξ is the spatial lag variable and $\tau_i = i\,T$ is the discrete lag time.

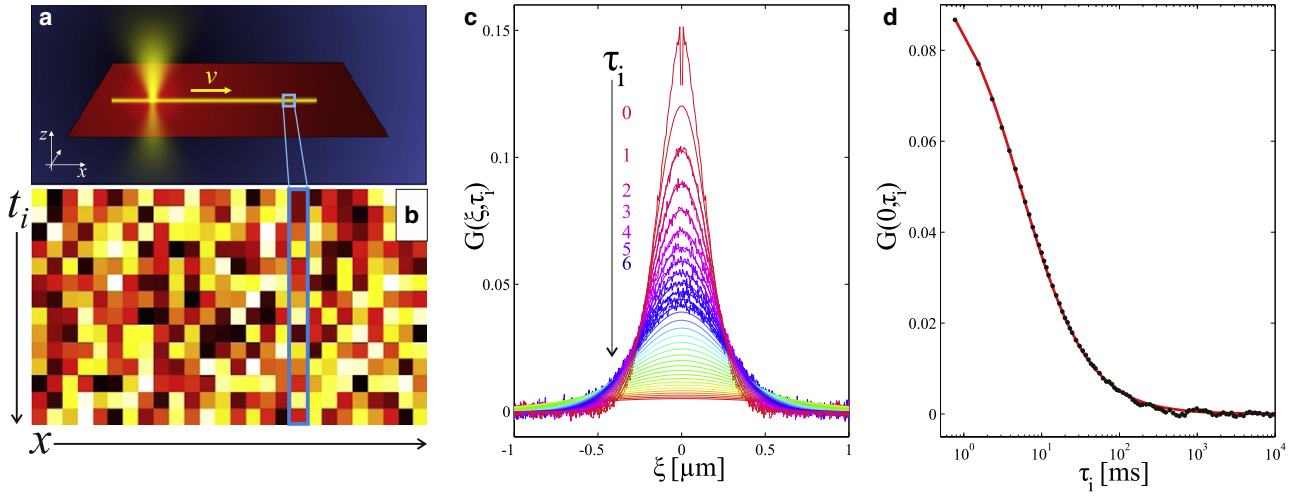

FIGURE 1 Principle of line-scan FCS. (*a*) A line is repeatedly scanned with a constant velocity v in the membrane. (*b*) Line scans can be arranged to form a pseudo-image where the vertical axis denotes the time. (*c*) Typical spatiotemporal correlation curves $G(\xi, \tau_i)$ with global fit to Eq. 2. Triplet contributions and afterpulsing cause the strong deviation of the fit for $G(\xi, 0)$. (*d*) Temporal correlation curve $G(0, \tau_i)$ constructed from a column of the pseudo-image (box in *a* and *b*) and fit to Eq. 3. Sample: Supported lipid bilayer composed of DOPC/Cholesterol/BodChol 1:1.5:10^{-4}. Laser power 35 μW, measurement time 100 s, $v = 0.034$ m/s.

With the assumption that the diffusion of the molecules in the membrane is not influenced by the scanning laser beam and that the spatial pixel size s is much smaller than the waist w_0 of the Gaussian detection area $\Omega(x, y) = \exp(-2(x^2 + y^2) / {w_0}^2)$, the spatiotemporal correlation function for one diffusing species can be calculated (17):

$$G(\xi, \tau_i) = \frac{1}{C\pi w_0^2}\exp\left[-\frac{\xi^2}{w_0^2 + 4D(\tau_i + \xi/v)}\right] \times \left(1 + \frac{4D}{w_0^2}\left(\tau_i + \frac{\xi}{v}\right)\right)^{-1}. \quad (2)$$

The spatial autocorrelation function $G(\xi, 0)$ corresponds to the well-known two-dimensional flow-diffusion model and a Gaussian detection area. Since the detection volume is scanned at a constant speed and the photon arrival times are recorded, $s << w_0$ can be fulfilled by selecting a sufficiently small bin time.

Typical correlation functions $G(\xi, \tau_i)$ are plotted in Fig. 1 *c*. Their dependence on the spatial lag variable ξ reflects the shape and size of the detection area. The decay of the amplitude and the broadening with τ_i is due to the diffusion of the molecules. Therefore, the diffusion coefficient D, the concentration of the fluorophores C, and also the waist of the detection area w_0 can be obtained directly by fitting the experimental correlation curve to the spatiotemporal correlation function in Eq. 2. A calibration measurement to determine the size of the detection area is thus not necessary. The velocity v, necessary to fit the data, can be determined with a high accuracy by scanning over a grid.

In contrast to spatiotemporal image correlation spectroscopy (22), where usually a few hundred frames are evaluated, in line-scan FCS typically 10^4–10^5 line scans are acquired. It is computationally complex to calculate the full correlation (Eq. 1) with a high spatial resolution. In addition, at large τ_i, the correlation curves $G(\xi, \tau_i)$ exhibit strong relative noise and carry less and less information about the waist and the diffusion coefficient. Therefore we propose to calculate $G(\xi, \tau_i)$ with a high spatial resolution only for a limited range of spatial lag variables ξ and for a limited number of lag times τ_i. To capture the statistical information at larger lag times, the temporal autocorrelation curve $G(0, \tau_i)$, calculated on a logarithmic scale with a multiple τ-algorithm, can be included in the evaluation (Fig. 1 *d*). Here, the choice of a pixel size $s \approx w_0$ leads to a correlation curve which exhibits much less statistical noise than for $s << w_0$. The correct model, which takes into account the finite size of the pixel, is (19,27)

$$G(0, \tau_i) = \frac{1}{C\pi s^2}\left(\sqrt{\pi}\mu_i \operatorname{erf}(\mu_i) + e^{-\mu_i^2} - 1\right) \quad \text{with } \mu_i = \frac{s}{\sqrt{w_0^2 + 4D\tau_i}}. \quad (3)$$

Equations 2 and 3 are valid for any diffusion coefficient. Very fast diffusion (diffusion time $\tau_D = {w_0}^2/4D$ comparable to the transit time due to scanning $t_s = w_0/v$) changes the shape of the spatial correlation curve $G(\xi, 0)$ considerably and can, in principle, be measured with line-scan FCS (17). However, the amplitudes of the spatiotemporal correlation curves then decrease rapidly with τ_i, which greatly limits the statistical accuracy. Therefore, line-scan FCS is best suited to study moderate-to-slow diffusion as found in lipid bilayers where the diffusion time is not much smaller then the repetition time T of the line-scan.

In raster image correlation spectroscopy, individual line-scans of a two-dimensional image are correlated (17). However, only if two line-scans overlap, they give rise to a significant correlation. Since the lines are separated by a distance equal to the pixel size s, the number of usable spatio-temporal correlation curves is limited to $\approx w_0/s$ for slowly diffusing molecules. This is not the case in line-scan FCS, where the same part of the membrane is sampled over and over again. This significantly enlarges the statistical accuracy, especially for fast sampling or slow diffusion.

Even for low laser powers, photobleaching can lead to a depletion of fluorophores. Measurements in a quasi-steady state after an initial bleaching period result in too low apparent concentrations. Due to the limited replenishment in the two-dimensional geometry, this is a general problem in membrane FCS, but it is especially severe for a reservoir of limited size. The system then can no longer reach a steady state, and the decaying intensity trace leads to seriously distorted correlation curves (*simulated curves* in Fig. 2). Here we present a novel scheme to correct for depletion due to photobleaching, not only applicable to line-scan FCS, but to FCS and image correlation spectroscopy in general. In contrast to previous correction schemes (28), it allows to extract correct concentrations from the measurement. This correction was essential to perform accurate measurements in lipid microdomains in phase separating bilayers (see Fig. 4 *a*) and can avoid a reduction of the measured concentration as is present in Fig. 3 *a*.

To correct for depletion, the slow decay of the intensity trace $F(t_i) = \langle F(x, t_i)\rangle_x$ (here $\langle\rangle_x$ denotes the average over one line scan) is first approximated by an analytical function $f(t)$. For an isolated reservoir, the decay can be assumed exponential: $f(t) = f_0 e^{-t/t_b}$. If the reservoir is connected weakly to a larger reservoir, a multiexponential is a good choice, but often two exponentials are sufficient. With the knowledge of $f(t)$, the intensity trace can be corrected before calculating the correlation curves. We propose the following transformation for the full intensity trace to correct for depletion, since it leads to a constant mean value and a constant variance of $F(t)$ with time, assuming a Poisson distribution for the number of particles in the detection volume:

$$F^c(x, t_i) = \frac{F(x, t_i)}{\sqrt{f(t_i)/f(0)}} + f(0)\left(1 - \sqrt{f(t_i)/f(0)}\right). \quad (4)$$

The corrected intensity trace $F^c(x, t_i)$ is not distinguishable from that of a system in a steady state. The correlation curve

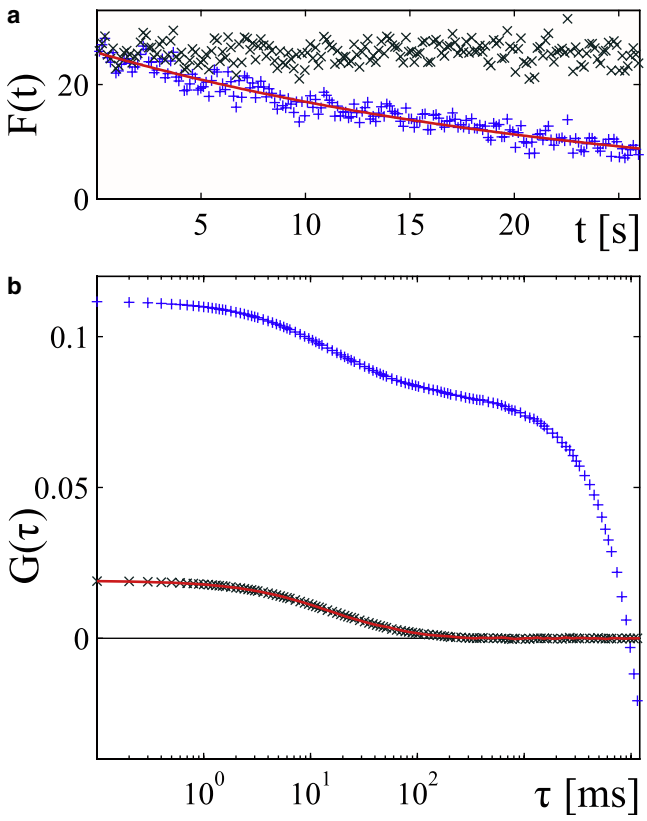

FIGURE 2 Correction for depletion due to photobleaching. (*a*) Simulated intensity trace (+), exponential fit (*solid line*), and corrected intensity trace (×). (*b*) Simulated correlation curves without (*solid line*) and with photobleaching (+) and corrected correlation curve (×). Correlation curves are averages of 16 simulations. Simulation parameters: $D = 1\ \mu m^2/s$, $w_0 = 0.25\ \mu m$, $p_{bl} = 1.2\ s^{-1}$, simulation time: 16×26 s.

$G(\xi, \tau_i)$, calculated from this corrected intensity trace, is not distorted any more by the decaying fluorescence and the concentration inferred by fitting is the initial concentration.

The effect of the bleaching correction is illustrated in Fig. 2 with simulated correlation curves. Even for strong bleaching, a distortion of the correlation curve is avoided. The corrected correlation curve coincides perfectly well with the correlation curve without photobleaching. Note that, in addition to depletion, photobleaching of fluorophores in the detection area can lead to an apparent reduction in the diffusion time, which is not corrected for with this approach. However, this effect is greatly reduced in line-scan FCS compared to standard confocal FCS (compare Fig. 3 *a*).

Even minor inhomogeneities, such as those often found in cellular membranes, can distort the correlation curve. The subtraction of a time-averaged line profile to obtain the fluctuations $\delta F^c(x, t_i)$, needed to calculate the correlation curve $G(\xi, \tau_i)$ with Eq. 1, already significantly reduces these artifacts (17,22):

$$\delta F^c(x, t_i) = F^c(x, t_i) - \langle F^c(x, t_i) \rangle_{t_i}. \quad (5)$$

In case the inhomogeneities are not constant in time, an intensity trace $\tilde{F}^c(x, t_i)$ smoothed in time, calculated for instance by convoluting $F(x, t_i)$ with a Gaussian, can be used to obtain $\delta F^c(x, t_i)$:

$$\delta F^c(x, t_i) = F^c(x, t_i) - \tilde{F}^c(x, t_i). \quad (6)$$

This approach is approximate but, for complex systems, it allows for meaningful fitting and thus extends the applicability of scanning FCS. However, stronger inhomogeneities might still influence the parameter estimates. Spatial features, much larger than the optical resolution (e.g., different domains of phase separating bilayers), should be evaluated separately.

The position of the sample has to be constant within the measurement time (at least a few seconds). Otherwise, horizontal drifts with speed V will appear as an additional flow component if the timescale w_0/V is comparable to the diffusion time τ_D; large vertical drifts will lead to undefined detection areas and distortions of the correlation curves.

MATERIALS AND METHODS

Optical setup

Measurements were performed on an laser scanning microscope (LSM) Meta 510 system (Carl Zeiss, Jena, Germany) using a 40 × NA 1.2 UV-VIS-IR C Apochromat water-immersion objective, the 488 nm-line of the Argon-Ion laser, and a homebuilt detection unit at the fiber output channel. A bandpass filter (HQ530/60, AHF Analyze Technik, Tübingen, Germany) was used behind a collimating achromat to reject the residual laser and background light. Another achromat (LINOS Photonics, Göttingen, Germany) with a shorter focal length was used to image the internal pinhole onto the aperture of the fiber connected to the avalanche photo diode (PerkinElmer, Boston, MA). The photon arrival times were recorded in the photon mode of the hardware correlator Flex 02-01D (Correlator.com, Bridgewater, NJ).

The correction collar of the objective was adjusted by maximizing the fluorescence intensity during a continuous line-scan while focusing on the plane of the membrane

The movement of the detection volume was controlled directly with the Zeiss LSM operation software, the linear scan path being selected in an LSM image. Depending on the system, the length of the scans was chosen between 10 μm and 30 μm. This is ~100-times the waist w_0 and leads to a similar gain in statistical accuracy due to parallel acquisition.

For optimal time resolution, the maximal repetition rate (1.3 kHz) was chosen. In this mode, the scan speed v was found to be constant at the central 70% of the field of view, which was exclusively used for data analysis. The nominal scan speed displayed by the LSM operation software coincided very well with the real one, as was determined by scanning over a grid (Ronchi ruling, Edmund Optics, Blackwood, NJ). If linearly polarized light is focused by a high numerical aperture objective, the resulting focus is elliptical (29). Since line-scan FCS relies on a rotational symmetric laser focus, a quarter-wave-plate (Melles Griot, Rochester, NY) was added in the beam path to generate excitation light with circular polarization.

An objective heater (Bioptechs, Butler, PA) was employed to control the temperature of the objective, thermally decoupled from the microscope by a plastic adaptor, and thus, control the temperature of the sample. Data were acquired when the temperatures measured on the objective and directly in the buffer above the membrane coincided.

Data analysis

Data analysis was performed with software written in MatLab (The MathWorks, Natick, MA). In case no correction was necessary, spatiotemporal correlation curves $G(\xi, \tau_i)$ were calculated based on the raw data of photon

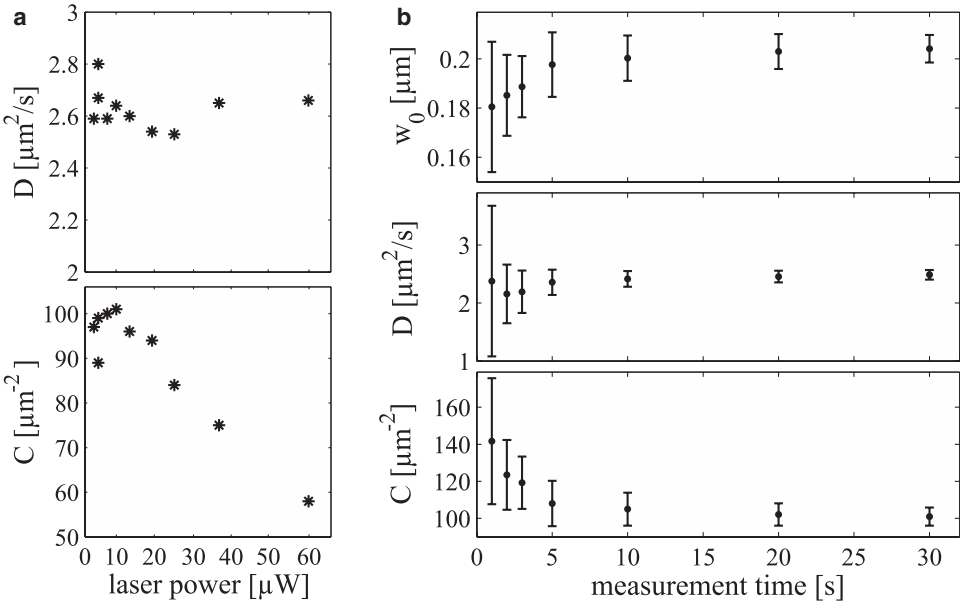

FIGURE 3 (*a*) Intensity series. Spatiotemporal correlation curves were measured at different laser powers ranging from 2.6 μW to 60 μW. The diffusion coefficient D displays virtually no dependence on the laser power and has a spread of only 3%. Depletion due to photobleaching causes a drop in the concentration C for higher laser powers. Measurement parameters: $v = 0.034$ m/s, acquisition time 100 s. Sample: Supported lipid bilayer composed of DOPC/Cholesterol/BodChol 1:1.5:10^{-4}. (*b*) Dependence of accuracy of parameter estimates on the measurement time. One measurement of 100 s (laser power 13 μW) was divided into independent measurements of 1, 2, 3, 5, 10, 20, and 30 s. Error bars denote the standard deviation of the parameter estimates.

arrival times with a time resolution of 0.15 μs. This leads to a pixel size of $s \approx 5$ nm and therefore to $s << w_0$, as required for Eq. 2. The spatial range was restricted to $\xi = -1.5\ \mu\text{m} \cdots +1.5\ \mu\text{m}$ and the temporal range to $\tau_i = \tau_1 \cdots \tau_{50}$ to limit the computation time.

When necessary, depletion and inhomogeneities were corrected for using Eqs. 4 and 6. Spatiotemporal correlation curves were calculated directly with Eq. 1 based on the corrected intensity fluctuations $\delta F^c(x, t_i)$ with a time resolution of 0.5 μs (pixel size $s \approx 20$ nm), also here for a limited range of ξ and τ_i.

The temporal correlation curve $G(0, \tau_i)$ was calculated based on a depletion-corrected coarse pseudo-image $F^c(x, t_i)$ (bin time 6 μs) using a multiple τ-algorithm.

The spatiotemporal correlation curve $G(\xi, \tau_i)$ and the temporal correlation curve $G(0, \tau_i)$ were fitted globally with Eqs. 2 and 3 using a weighted nonlinear least-squares fitting algorithm to result in estimates for the concentration C, the diffusion coefficient D, and the waist w_0. On a standard personal computer (2.3 GHz) the calculation and fitting of a spatiotemporal correlation curve takes ~5 min.

On phase-separating bilayers, correlation curves were calculated independently for the different lipid phases. The phases could be identified due to the different affinity of the fluorescent dye to the L_o- and the L_d-phases. During the global fit, the waist w_0 was assumed to be the same in both phases.

Materials

1,2-dioleoyl-*sn*-glycero-3-phosphocholine (dioleoylphosphatidylcholine; DOPC), n-stearoyl-d-erythrosphingosylphosphorylcholine (sphingomyelin, SM), brain sphingomyelin, and cholesterol were purchased from Avanti Polar Lipids (Alabaster, AL) and used without further purification. Cholesteryl 4,4-difluoro-5,7-dimethyl-4-bora-3a,4a-diaza-s-indacene-3-dodecanoate (cholesteryl BODIPY FL C_{12}, BodChol) and n-4,4-difluoro-5,7-dimethil-4-bora-3a,4a-diaza-s-indacene-3-pentanoylsphingosine (BODIPY FL C5-ceramide, BodCer) were purchased from Molecular Probes (Eugene, OR). Poly-L-lysine was obtained from Sigma (St. Louis, MO).

Preparation of supported lipid bilayers

Planar-supported bilayers were prepared as follows (30): lipids with molar ratios as indicated were dissolved in chloroform and evaporated first under nitrogen flux and then under vacuum for 1 h. The lipids were then rehydrated with 150 mM NaCl, 3 mM $CaCl_2$, and 10 mM HEPES buffer (pH 7.4) and resuspended by vigorous vortexing. The suspension was bath-sonicated at 60°C for 1 h to obtain small unilamellar vesicles. One hundred microliters were then placed on a freshly cleaved mica substrate glued to a glass coverslip, for 30 min at 60°C. Before slow cooling to room temperature, the sample was rinsed several times to remove unfused vesicles.

Preparation of supported plasma membrane patches

Supported plasma membrane patches were prepared according to a protocol adapted from Perez et al. (31). Briefly, HEK-293T cells were grown in Dulbecco's Modified Eagle Medium (cat. No. 41965, Invitrogen, Carlsbad, CA) with 10% fetal calf serum (Cambrex, East Rutherford, NJ) in uncoated petri dishes. Osmotic swelling of the cells was induced for 3 min with 1 mM $MgCl_2$, 1.8 mM $CaCl_2$ solution. Polylysine-coated cover slides were placed on the cells for 5 min using moderate pressure, removed carefully, washed with phosphate-buffered saline, and mounted in the JPK BioCell sample holder (JPK Instruments, Berlin, Germany). Membrane patches were labeled with BodCer in micromolar concentration for a few minutes at 40°C and subsequently washed.

For experiments with GFP-GPI, 293T cells were seeded on Fibronectin-coated coverslips and were transfected with pGFP-GPI DNA using Lipofectamine 2000 (Invitrogen). Cells reached 80% confluency on the following day, when rip-off experiments were performed.

RESULTS AND DISCUSSION

Spatiotemporal correlation curve

Fig. 1, *b* and *c*, show experimental correlation curves together with the global fit to Eqs. 2 and 3. Note that the spatial autocorrelation curve $G(\xi, 0)$ deviates strongly from the fit, especially for small lag-variables. Due to the scanning, these small lag-variables correspond to small lag-times in the μs range where contributions from triplet kinetics and after-pulsing from the detectors are strong (32). These artifacts could be accounted for using a refined model, but since they are not present in the correlation curves $G(\xi, \tau_i)$ for $\tau_i > 0$, a simple choice is to exclude $G(\xi, 0)$ from the fit.

Photobleaching and measurement times

In standard confocal FCS, the long residence time of the fluorophores in the detection area leads to strong photobleaching, even for moderate laser powers. This results in a systematic error in the diffusion coefficients toward larger values. In line-scan FCS, the residence time is greatly reduced. Therefore photobleaching has virtually no effect on the measured diffusion coefficients, as can be seen in Fig. 3 *a* for laser powers between 2.6 μW (usually used for FCS on membranes) and 60 μW (strong even for measurements on small dye diffusing fast in solution). Note the high reproducibility of line-scan FCS: the measured diffusion coefficients scatter only by 3%. Since the data acquisition was started after an initial bleaching period, when the system was in a quasi-steady state, the depletion correction resulted in reduced concentrations at the beginning of the data acquisition. This is the cause for the strong decrease of the measured concentrations with higher laser powers.

The high excitation intensities applicable in line-scan FCS permit accurate measurements within minimal acquisition times. To investigate the effect of the measurement time on the accuracy of the parameter estimates, we divided one long measurement into several individual short measurements and plotted the parameters obtained from the fit as a function of the new measurement time (Fig. 3 *b*). Although a measurement time of 1 s was clearly not enough, 5 s already resulted in quite small spreads of the parameter estimates. The gain in accuracy from 10 s to 30 s is small. Probably, in this regime, the systematic errors like instabilities or inhomogeneities in the membrane limit the accuracy. Therefore, longer measurement times are not needed. For very short measurement times, the correlation curves are very noisy and lack statistical accuracy, which leads to a systematic error in the inferred waist and concentration.

Dynamics in phase-separating model membranes

Different mixtures of sphingomyelin, cholesterol, and unsaturated phosphatidylcholine, commonly referred to as raft mixtures, are typical models to study the lateral organization of membrane components related to putative phase separation in cell membranes (33–35). Nevertheless, the length and saturation degree of lipid acyl chains, as well as the relative ratios of the components, strongly influence the physical properties of the membranes (36,37). We used line-scan FCS to study the diffusion coefficients and partition coefficients in three typical phase-separating lipid mixtures which contain sphingomyelin of different sources (i.e., varying acyl chains) and different sphingomyelin/cholesterol ratios (36,38,39). To this end, the line was scanned through both phases of interest, and parts belonging to each phase, identified by the different concentration of the fluorescent cholesterol analog BodChol, were analyzed independently (see Fig. 4 *c*). This specific fluorescent probe was chosen since it partitions considerably into both the L_o and L_d phase and does not exhibit strong electrostatic interactions with the support (38). It is interesting to point out that a different fluorescent cholesterol analog would have been more suitable if the behavior of unlabeled sterols was to be studied (23,40).

The results are summarized in Fig. 4 and are consistent with values obtained with a two-focus scanning FCS approach (38). In addition, discrepancies between these values and those found with complementary techniques (41) could be attributed to differences in the choice of lipid probes (e.g., electric charge) and the method of bilayer preparation (e.g., tethered versus mica-supported, symmetric versus asymmetric bilayers). The increase of the SM C18:0/Chol ratio from 1:1 to 1:0.7 (composition *a* to *b*, as defined in Fig. 4) results in a threefold decrease in diffusion in the L_o (liquid-ordered) phase. The L_d (liquid-disordered) phase is hardly affected, since cholesterol is mainly enriched in the L_o phase where it decreases the translational order (42). Substituting C18:0 sphingomyelin with brain sphingomyelin (composition *b* to *c*, as in Fig. 4) causes an increase in the diffusion coefficient in both phases, but especially in the L_o phase. This may be due to the partition of the unsaturated sphingomyelin fraction into the L_d phase resulting in a lower SM/Chol ratio in the L_o phase. Furthermore, unsaturated sphingomyelin may

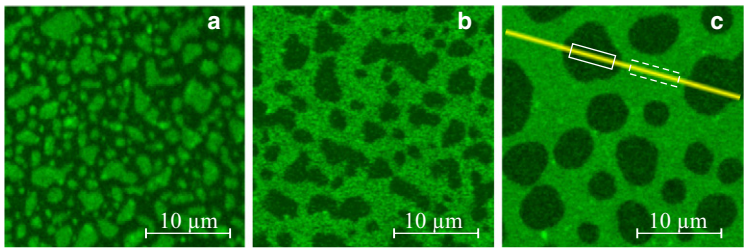

Composition	Diffusion coefficient		Partition coefficient	
	D_{ld} [$\mu m^2/s$]	D_{lo} [$\mu m^2/s$]	C_{lo}/C_{ld} (FCS)	F_{lo}/F_{ld} (Intensity)
a	4.9 ± 0.5	0.43 ± 0.03	0.190 ± 0.009	0.100 ± 0.003
b	3.7 ± 0.5	0.13 ± 0.02	0.218 ± 0.018	0.101 ± 0.006
c	6.2 ± 0.4	0.42 ± 0.02	0.330 ± 0.008	0.175 ± 0.003

FIGURE 4 Phase-separating model membranes. (*a*) DOPC/SM C18:0/Chol 1:1:1; (*b*) DOPC/SM C18:0/Chol 1:1:0.7; (*c*) DOPC/brain SM/Chol 1:1:0.7. Fluorescent marker: 0.004 mol % BodChol. Temperature 22°C. Table: results from line-scan FCS. Measurement parameters: $v = 0.034$ m/s, acquisition time 100 s, laser power 5 μW. At least 10 measurements on two different samples per composition. In panel *c*, a typical scan path is shown together with the parts analyzed for the L_d-phase (*dashed line*) and the L_o-phase (*solid line*).

simply perturb the local packing in the L_o phase (43), in line with the observed increase in the diffusion coefficient and partition of bulky fluorophores in the ordered phase.

These results show, on one hand, that dynamics and partition of membrane components are strongly influenced by the exact lipid composition and particular caution should be used when deriving general conclusions from specific model systems. On the other hand, the results in Figs. 3 and 4 clearly demonstrate that the novel FCS implementation presented here has the high accuracy needed to appreciate the small changes in physical parameters involved in lipid-lipid interactions. Furthermore, the novel correction for depletion due to photobleaching was vital for accurate concentration measurements, especially for sample *a* (Fig. 4), which exhibits small bright L_d domains in the L_o matrix. Due to the slow exchange of the dye between the two phases, the L_d domains act effectively as small reservoirs, prone to fast depletion. However, the lipid exchange is still significant, as can be deduced from the absence of complete depletion (data not shown).

Finally, due to photoselection and the influence of the microenvironment on the photophysical properties of the fluorophore, the molecular brightness is higher in the L_d phase than in the more rigid L_o phase. Partition coefficients obtained just by imaging are therefore inaccurate. According to our results in Fig. 4, the parameters calculated from the fluorescence intensities had errors as large as 100%. Only FCS, which directly measures concentrations, results in the correct partition coefficients.

Diffusion in plasma membrane patches

To test line-scan FCS on biological samples, we performed diffusion measurements on cellular membrane patches. For data acquisition, homogeneous parts were chosen in the LSM-image (Fig. 5 *c*). However, small residual inhomogeneities were still present and required correction with Eq. 6. For membrane patches stained with BodCer we found a diffusion coefficient of $D = 0.33 \pm 0.07\ \mu m^2/s$ at 27°C. We also measured diffusion in patches prepared from cells transfected with a GPI-GFP construct. The GPI-GFP diffused slightly faster than the BodCer with $D = 1.1 \pm 0.3\ \mu m^2/s$ at 25°C. We found a significant spread among different patches and even different positions in one patch, larger than the reproducibility of the technique, indicating a strong heterogeneity. The average diffusion coefficients are comparable to values measured in the same system with single particle tracking (44) and to those obtained using FCS on the plasma membranes of living cells (7,45). The origin of the differences in the diffusion coefficients between BodCer and GPI-GFP remains unclear but a possible explanation might result, e.g., from the localization of the two probes in the different membrane leaflets.

Temperature dependence of membrane viscosity

The temperature dependence of diffusion coefficients can give new insights into the lipid-lipid interactions. The diffusion of lipids and proteins can be well described by so-called free-volume theories (46). In contrast to continuous hydrodynamic theories which can be used to describe diffusion of larger objects, these descriptions take into account the discrete nature of lipids in a membrane and assume diffusion of a molecule to take place only when there is a free space in close vicinity. The energy required to hop into an available free volume is the activation energy E_a. It takes into account the interactions of a lipid molecule with its neighbors in the bilayer, the interaction with the surrounding fluid or surfaces, and also the energy required to create a hole next to the

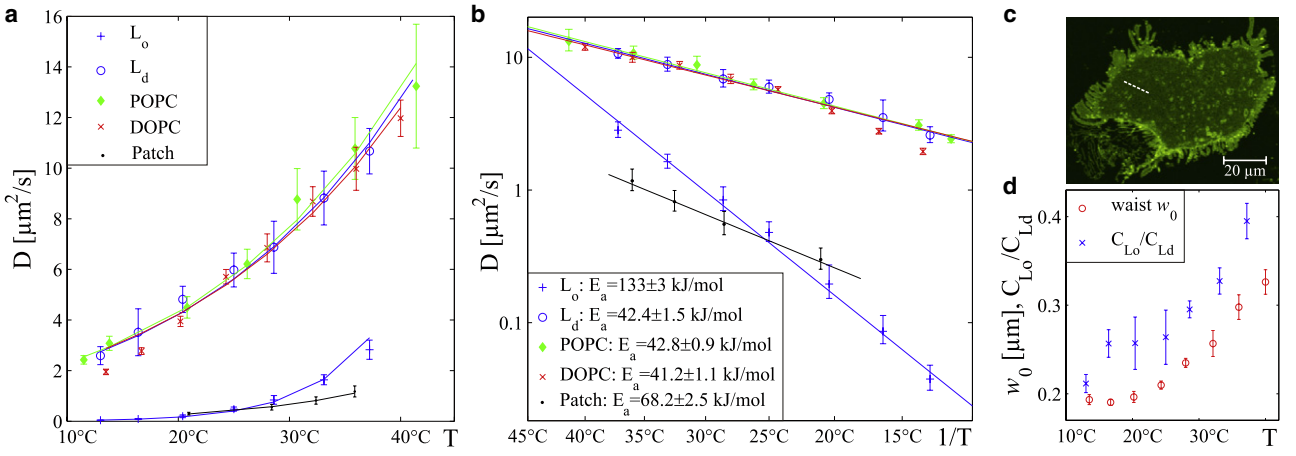

FIGURE 5 Temperature dependence of diffusion in model membranes. (*a*) Temperature dependence of the diffusion coefficient of BodChol in supported lipid bilayers composed of DOPC/brain SM/cholesterol 1:1:0.7, POPC and DOPC, and of BodCer in cellular plasma membrane patches. Solid lines indicate fits to the Arrhenius equation (Eq. 7). (*b*) Plot of log(*D*) versus 1/*T* for all samples considered in *a*) and robust linear fits to infer the activation energies. (*c*) LSM-image of cellular membrane patch. Line-scan FCS was performed on parts with low inhomogeneities. (*Dashed line*) Typical part of the scan used to construct the correlation curves. (*d*) Temperature dependence of the partition coefficient C_{lo}/C_{ld} in the phase-separating lipid bilayer and of the waist w_0, indicating optical aberrations with higher temperature. Measurement parameters: $v = 0.034$ m/s, acquisition time 50 s, laser power 13 μW, at least five measurements per data point.

diffusing molecule, whenever this event is locally associated with an energy change (46). The temperature dependence of diffusion is described by the Arrhenius equation:

$$D = D_0 e^{-E_a/RT}. \quad (7)$$

The study of this temperature dependence with optical methods is severely complicated by temperature-induced aberrations. For this reason, the number of studies addressing this issue is limited. Since line-scan FCS is not affected by these aberrations, we could employ it to investigate the temperature dependence of diffusion coefficients in several lipid membranes. To ensure a well-defined temperature in the sample, we used an objective heater and measured the temperature directly in the buffer above the sample. The results are shown in Fig. 5 *a*. In Fig. 5 *b*, the same data are plotted as log(D) versus $1/T$. The linear dependence of the data points is clearly visible and suggests that Eq. 7 provides a valid description. Interestingly, the diffusion coefficients and activation energies of BodChol in DOPC, palmitoyloleoylphosphatidylcholine (POPC), and in the L_d phase of a DOPC/brain SM/cholesterol 1:1:0.7 bilayer have essentially the same value, probably resulting from being in a similar physical state, independently of lipid acyl-chain composition. Fillipov et al. (47) also found an identical behavior for DOPC and POPC in a slightly different system using pulsed field gradient nuclear magnetic resonance, albeit with a 30% lower activation energy. The diffusion coefficient in the L_o phase of the phase-separating bilayer was very low at 15°C, but it increased dramatically with the temperature due to a threefold higher activation energy, pointing to a much higher degree of lipid-lipid interaction. For example, going from room temperature (22°C) to physiological temperatures (37°C) increases the diffusion coefficient by more than one order of magnitude. On the contrary, the rest of the membrane (L_d phase) is much less influenced by the change in temperature (twofold change in the diffusion coefficient). As a consequence, our results suggest that particular care has to be taken in controlling the temperature in quantitative studies of membrane dynamics. This should also be considered when studying the lateral organization of the plasma membrane in vivo: temperatures below physiological temperatures (i.e., 25°C or 4°C) might have in fact significant effects on the physical properties of putative ordered cholesterol-enriched microdomains.

The activation energy in cellular membrane patches is slightly higher than that of the L_d phase and the diffusion coefficient at room temperature is comparable to that of the L_o phase. Here the data of only one specific patch are shown as an example, the heterogeneity between different patches being significant (~50%). A direct comparison with more simple systems is made difficult by the fact that the plasma membrane has a very complex lipid composition. In addition, the diffusion behavior of fluorescent lipids might be influenced by the high concentration of proteins, some of which interact strongly with the supporting surface, the presence of some residual cytoskeleton, and the physical properties of the fluorophore itself.

Not only the diffusion coefficient but also the partition coefficient in phase-separating bilayers depends on the temperature (Fig. 5 *d*). This reflects the perturbation of lipid packing in the L_o phase as a consequence of increased thermal energy.

Note that the size of the detection area increases significantly above room temperature (Fig. 5 *d*). The objective is not designed for such temperatures and the adjustment of the correction collar reduces the aberrations only partially. Confocal FCS measurements not taking the enlarged detection volume into account would have resulted in an almost threefold error of D at 45°C. Since line-scan FCS is a calibration-free technique, these aberrations only lead to a weaker signal with higher temperature, but they do not induce any further error in the measured parameters.

CONCLUSION

Line-scan FCS features an excellent spatial and temporal resolution, perfectly suited to study dynamics in membranes with low curvature like very large vesicles or supported artificial or cellular membranes. Similar to spatiotemporal image correlation spectroscopy, parallel acquisition greatly increases the statistical accuracy. However, by concentrating on one line, even fast membrane diffusion and possibly slow solution diffusion can be measured accurately within very short measurement times. A further increase in temporal resolution, sufficient to study fast solution diffusion, would require repetition rates faster than implemented in standard laser scanning microscopes.

Line-scan FCS is insensitive to photobleaching and provides absolute values for diffusion coefficients without the need for a calibration measurement to determine the size of the detection area. Concentrations of membrane components can be precisely measured, independent of local brightness variations, and in very viscous domains, similar to those found in cellular membranes, as well. Therefore, this technique eliminates the main experimental difficulties usually connected with confocal FCS on membranes, like photobleaching, long measurement times limited by instabilities, exact vertical positioning, and calibration of the detection volume. Furthermore, correction schemes for depletion of fluorophores and minor inhomogeneities extend the use of line-scan FCS to more demanding biological samples.

We applied line-scan FCS to investigate the diffusion and partition behavior of fluorescent lipids in three commonly used phase-separating bilayers and to probe the temperature dependence of diffusion in several model membranes and in cellular plasma membrane patches. Our results show that the physical properties of the liquid ordered phase—as a model for cellular rafts—are strongly influenced by 1), the specific chemical composition of the bilayer; and 2), by the

temperature, due to the high activation energy of this lipid phase. Furthermore, line-scan FCS appears to be the method of choice in measuring, within seconds, accurate diffusion coefficients and concentrations in planar membranes, also in challenging experimental conditions.

The simple implementation with laser-scanning microscopes, preferably with single photon detectors, will promote line-scan FCS as a standard method to study membrane dynamics.

We acknowledge Horst Vogel and Christophe Danelon for help in sample preparation and Zdenek Petrasek for help with the manuscript.

This work was supported by the Max Planck Society, Munich, Germany.

REFERENCES

1. Rigler, R., and E. Elson. 2001. Fluorescence Correlation Spectroscopy: Theory and Applications. Springer, New York.
2. Bacia, K., and P. Schwille. 2003. A dynamic view of cellular processes by in vivo fluorescence auto- and cross-correlation spectroscopy. *Methods*. 29:74–85.
3. Enderlein, J., I. Gregor, D. Patra, T. Dertinger, and U. B. Kaupp. 2005. Performance of fluorescence correlation spectroscopy for measuring diffusion and concentration. *ChemPhysChem*. 6:2324–2336.
4. Kahya, N., and P. Schwille. 2006. Fluorescence correlation studies of lipid domains in model membranes. *Mol. Membr. Biol*. 23:29–39, [Review].
5. Bates, I. R., P. W. Wiseman, and J. W. Hanrahan. 2006. Investigating membrane protein dynamics in living cells. *Biochem. Cell Biol*. 84:825–831.
6. Meacci, G., J. Ries, E. Fischer-Friedrich, N. Kahya, P. Schwille, et al. 2006. Mobility of Min-proteins in *Escherichia coli* measured by fluorescence correlation spectroscopy. *Phys. Biol*. 3:255–263.
7. Bacia, K., D. Scherfeld, N. Kahya, and P. Schwille. 2004. Fluorescence correlation spectroscopy relates rafts in model and native membranes. *Biophys. J*. 87:1034–1043.
8. Kahya, N., D. Wiersma, B. Poolman, and D. Hoekstra. 2002. Spatial organization of bacteriorhodopsin in model membranes light-induced mobility changes. *J. Biol. Chem*. 277:39304–39311.
9. Pramanik, A., and R. Rigler. 2001. Ligand-receptor interactions in the membrane of cultured cells monitored by fluorescence correlation spectroscopy. *Biol. Chem*. 382:371–378.
10. Ries, J., and P. Schwille. 2008. New concepts for fluorescence correlation spectroscopy on membranes. *Phys. Chem. Chem. Phys*. 10:3487–3497.
11. Petersen, N. 1986. Scanning fluorescence correlation spectroscopy. I. Theory and simulation of aggregation measurements. *Biophys. J*. 49:809–815.
12. Petersen, N., D. Johnson, and M. Schlesinger. 1986. Scanning fluorescence correlation spectroscopy. II. Application to virus glycoprotein aggregation. *Biophys. J*. 49:817–820.
13. Meyer, T., and H. Schindler. 1988. Particle counting by fluorescence correlation spectroscopy. Simultaneous measurement of aggregation and diffusion of molecules in solutions and in membranes. *Biophys. J*. 54:983–993.
14. Berland, K., P. So, Y. Chen, W. Mantulin, and E. Gratton. 1996. Scanning two-photon fluctuation correlation spectroscopy: particle counting measurements for detection of molecular aggregation. *Biophys. J*. 71:410–420.
15. Ruan, Q. Q., M. A. Cheng, M. Levi, E. Gratton, and W. W. Mantulin. 2004. Spatial-temporal studies of membrane dynamics: scanning fluorescence correlation spectroscopy (SFCS). *Biophys. J*. 87:1260–1267.
16. Xiao, Y., V. Buschmann, and K. Weston. 2005. Scanning fluorescence correlation spectroscopy: a tool for probing microsecond dynamics of surface-bound fluorescent species. *Anal. Chem*. 77:36–46.
17. Digman, M., C. Brown, P. Sengupta, P. Wiseman, A. Horwitz, et al. 2005. Measuring fast dynamics in solutions and cells with a laser scanning microscope. *Biophys. J*. 89:1317–1327.
18. Skinner, J., Y. Chen, and J. Muller. 2005. Position-sensitive scanning fluorescence correlation spectroscopy. *Biophys. J*. 89:1288–1301.
19. Ries, J., and P. Schwille. 2006. Studying slow membrane dynamics with continuous wave scanning fluorescence correlation spectroscopy. *Biophys. J*. 91:1915–1924.
20. Petrasek, Z., and P. Schwille. 2008. Precise measurement of diffusion coefficients using scanning fluorescence correlation spectroscopy. *Biophys. J*. 94:1437–1448.
21. Satsoura, D., B. Leber, D. Andrews, and C. Fradin. 2007. Circumvention of fluorophore photobleaching in fluorescence fluctuation experiments: a beam scanning approach. *ChemPhysChem*. 8:834–848.
22. Hebert, B., S. Costantino, and P. Wiseman. 2005. Spatiotemporal image correlation spectroscopy (STICS) theory, verification, and application to protein velocity mapping in living CHO cells. *Biophys. J*. 88:3601–3614.
23. Chiantia, S., J. Ries, G. Chwastek, D. Carrer, Z. Li, R. Bittman, et al. 2008. Role of ceramide in membrane protein organization investigated by combined AFM and FCS. *Biochim. Biophys. Acta*. 1778:1356–1364.
24. Rajendran, L., A. Schneider, G. Schlechtingen, S. Weidlich, J. Ries, et al. 2008. Efficient inhibition of the Alzheimer's disease β-secretase by membrane targeting. *Science*. 320:520–523.
25. Simons, K., and E. Ikonen. 1997. Functional rafts in cell membranes. *Nature*. 387:569–572.
26. Brown, D. 2001. Seeing is believing: visualization of rafts in model membranes. *Proc. Natl. Acad. Sci. USA*. 98:10517–10518.
27. Ries, J., E. P. Petrov, and P. Schwille. 2008. Total internal reflection fluorescence correlation spectroscopy: Effects of lateral diffusion and surface generated fluorescence. *Biophys. J*. 95:390–399.
28. Delon, A., Y. Usson, J. Derouard, T. Biben, and C. Souchier. 2004. Photobleaching, mobility, and compartmentalization: inferences in fluorescence correlation spectroscopy. *J. Fluoresc*. 14:255–267.
29. Dorn, R., S. Quabis, and G. Leuchs. 2003. The focus of light-linear polarization breaks the rotational symmetry of the focal spot. *J. Mod. Opt*. 50:1917–1926.
30. Chiantia, S., N. Kahya, and P. Schwille. 2005. Dehydration damage of domain-exhibiting supported bilayers: an AFM study on the protective effects of disaccharides and other stabilizing substances. *Langmuir*. 21:6317–6323.
31. Perez, J., K. Martinez, J. Segura, and H. Vogel. 2006. Supported cell-membrane sheets for functional fluorescence imaging of membrane proteins. *Adv. Funct. Mater*. 16:306–312.
32. Zhao, M., L. Jin, B. Chen, Y. Ding, H. Ma, et al. 2003. Afterpulsing and its correction in fluorescence correlation spectroscopy experiments. *Appl. Opt*. 42:4031–4036.
33. Rinia, H., M. Snel, J. van der Eerden, and B. de Kruijff. 2001. Visualizing detergent resistant domains in model membranes with atomic force microscopy. *FEBS Lett*. 501:92–96.
34. Filippov, A., G. Oradd, and G. Lindblom. 2004. Lipid lateral diffusion in ordered and disordered phases in raft mixtures. *Biophys. J*. 86:891–896.
35. Baumgart, T., G. Hunt, E. Farkas, W. Webb, and G. Feigenson. 2007. Fluorescence probe partitioning between L_o/L_d phases in lipid membranes. *Biochim. Biophys. Acta Biomembr*. 1768:2182–2194.
36. Kahya, N., D. Scherfeld, K. Bacia, B. Poolman, and P. Schwille. 2003. Probing lipid mobility of raft-exhibiting model membranes by fluorescence correlation spectroscopy. *J. Biol. Chem*. 278:28109–28115.
37. Li, X., J. Smaby, M. Momsen, H. Brockman, and R. Brown. 2000. Sphingomyelin interfacial behavior: the impact of changing acyl chain composition. *Biophys. J*. 78:1921–1931.
38. Chiantia, S., J. Ries, N. Kahya, and P. Schwille. 2006. Combined AFM and two-focus SFCS study of raft-exhibiting model membranes. *ChemPhysChem*. 7:2409–2418.

39. Lawrence, J., D. Saslowsky, J. Edwardson, and R. Henderson. 2003. Real-time analysis of the effects of cholesterol on lipid raft behavior using atomic force microscopy. *Biophys. J.* 84:1827–1832.

40. Hölttä-Vuori, M., R. -L. Uronen, J. Repakova, E. Salonen, I. Vattulainen, et al. 2008. BODIPY-cholesterol: a new tool to visualize sterol trafficking in living cells and organisms. *Traffic.* 9:1839–1849.

41. Kiessling, V., J. M. Crane, and L. K. Tamm. 2006. Transbilayer effects of raft-like lipid domains in asymmetric planar bilayers measured by single molecule tracking. *Biophys. J.* 91:3313–3326.

42. Simons, K., and W. Vaz. 2004. Model systems, lipid rafts, and cell membranes. 1. *Annu. Rev. Biophys. Biomol. Struct.* 33:269–295.

43. Filippov, A., G. Oradd, and G. Lindblom. 2006. Sphingomyelin structure influences the lateral diffusion and raft formation in lipid bilayers. *Biophys. J.* 90:2086–2092.

44. Nishimura, S., M. Vrljic, L. Klein, H. McConnell, and W. Moerner. 2006. Cholesterol depletion induces solid-like regions in the plasma membrane. *Biophys. J.* 90:927–938.

45. Lenne, P., L. Wawrezinieck, F. Conchonaud, O. Wurtz, A. Boned, et al. 2006. Dynamic molecular confinement in the plasma membrane by microdomains and the cytoskeleton meshwork. *EMBO J.* 25:3245–3256.

46. Almeida, P., and W. Vaz. 1995. Structure and dynamics of membranes: from cells to vesicles. *In* Lateral Diffusion in Membranes.. Elsevier, Amsterdam, The Netherlands.

47. Filippov, A., G. Oradd, and G. Lindblom. 2003. The effect of cholesterol on the lateral diffusion of phospholipids in oriented bilayers. *Biophys. J.* 84:3079–3086.